The Astronomical Journal, 140:1987–1994, 2010 December doi:10.1088/0004-6256/140/6/1987
© 2010. The American Astronomical Society. All rights reserved. Printed in the U.S.A.

A CATALOG OF 19,100 QUASI-STELLAR OBJECT CANDIDATES WITH REDSHIFT 0.5–1.5*

J. B. Hutchings[1] and L. Bianchi[2]
[1] Herzberg Institute of Astrophysics, 5071 West Saanich Road, Victoria, BC, V9E 2E7, Canada
[2] Department of Physics and Astronomy, Johns Hopkins University, 3400 North Charles Street, Baltimore, MD 21218, USA
Received 2010 March 18; accepted 2010 October 2; published 2010 November 10

ABSTRACT

We discuss a sample of ∼60,000 objects from the combined Sloan Digital Sky Survey–*Galaxy Evolution Explorer* (SDSS–*GALEX*) database with UV–optical colors that should isolate QSOs in the redshift range 0.5–1.5. We use SDSS spectra of a subsample of ∼4500 to remove stellar and galaxy contaminants in the sample to a very high level, based on the 7-band photometry. We discuss the distributions of redshift, luminosity, and reddening of the 19,100 QSOs (∼96%) that we estimate to be present in the final sample of 19,812 point sources. The catalog is available as an online table.

Key words: quasars: general

Online-only material: machine-readable and VO tables

1. INTRODUCTION AND SAMPLES

We have used the combined Sloan Digital Sky Survey–*Galaxy Evolution Explorer* (SDSS–*GALEX*) database to isolate and investigate samples of active galactic nuclei. Bianchi et al. (2010) describe in detail the general catalogs from which this sample has been extracted, but we review the essential procedures in the next paragraph. The seven-color wide wavelength base offers advantages in sample selection from ground-based-only photometric databases, and in this paper we investigate objects with UV and optical colors, which spectral templates indicate should be dominated by QSOs in the $z = 0.5$–1.5 redshift range. Bianchi (2009) and Bianchi et al. (2009) describe the templates used. Figure 1 shows how use of the FUV and NUV photometry from *GALEX* separates out QSOs in the redshift range 0.5–1.5 very cleanly from stars and normal galaxy populations. The reason that QSOs occupy this region of the diagram, almost exclusively, is that Lyα emission passes through the *GALEX* passbands. The two templates for normal and enhanced Lyα emission emphasize this fact and illustrate the range of FUV–NUV values, which is much larger than the photometric errors. This paper presents a sample of objects based on this separation that we argue contains QSOs at about the 96% level and samples the redshift range smoothly. We expect completeness to be high in the redshift range 0.8–1.0, and less so toward the edges of the 0.5–1.5 range.

Other publications that have used the SDSS magnitudes alone have yielded considerably larger samples and isolated higher redshift objects well (e.g., Richards et al. 2001, 2002, 2004, 2009; Fan et al. 2000). Those papers made earlier use of the g, r, i relationship, which we have noted (Hutchings & Bianchi 2008), and use in this paper too. While the catalog we describe here is smaller, because of its restricted redshift range and sky coverage, we show that it should have a high purity (fraction of QSOs), so that it can be used without the need for spectroscopic confirmation. It also includes the added spectral energy distribution (SED) information from the shorter rest wavelengths.

The candidates are selected from the source catalog of *GALEX* Medium Imaging Survey unique UV sources from data release GR5, matched to SDSS data release DR7, and restricted to sources with photometric error <0.3 in the FUV, NUV, and r bands. The Bianchi et al. (2010) catalog is also restricted to sources within the central 1° diameter of the *GALEX* field, to avoid artifacts and bad photometry. Since we are constructing a seven-color photometric sample, this restriction is important in ensuring only good photometry in the UV and overrides the requirements for making the sample as large or complete as possible in sky coverage. This selection process yields an area covered of 1103 deg^2.

The *GALEX* archive contains some objects observed more than once, so Bianchi et al. (2010) constructed a unique-source catalog as follows. *GALEX* sources were considered duplicates if their positions lie within 2.″5, unless the objects are from the same observation. The measurement from the longest NUV exposure was then used, and the other measurement was eliminated. The "unique" UV sources were then positionally matched with the SDSS DR7 "photoprimary" table (the SDSS catalog that contains only unique objects), using a match radius of 3″. A *GALEX* source may have multiple SDSS source matches because of the three-times higher spatial resolution of SDSS over *GALEX*. In such cases, the closest position match was retained. However, in order to use the full color information on sources, UV sources with multiple optical matches were excluded from the analysis. In the case of crowded fields, even if the match is correct, the UV colors may be affected by the poorer *GALEX* resolution. Because of these exclusions, if the catalog were to be used for estimating sky density of sources, a statistical correction should be applied, shown by Figure 3 and Table 2 of Bianchi et al. (2010). The fraction of sources with multiple matches is lowest at high Galactic latitudes, of the order of ⩽10%. Bianchi et al. (2010) also estimate the statistical probability of spurious matches, which is of the order of few percent, except near the Galactic plane (latitudes $|b| < 25°$) where it is higher.

The color–color region of the initial selected sample is shown in Figure 1, along with the stellar and QSO template plots. Only a few cool white dwarfs (see Bianchi et al. 2009; Figure 1) are expected as stellar contaminants in this region, according to stellar models. We initially included sources classified in SDSS as extended as well as point, in case these classifications are unreliable for faint objects. This selection gives us 22,993 point sources and 36,770 extended sources. Of these 4532 have

* This paper is based on archival data from the *Galaxy Evolution Explorer* (*GALEX*) which is operated for NASA by the California Institute of Technology under NASA contract NAS5-98034, and on data from the SDSS.

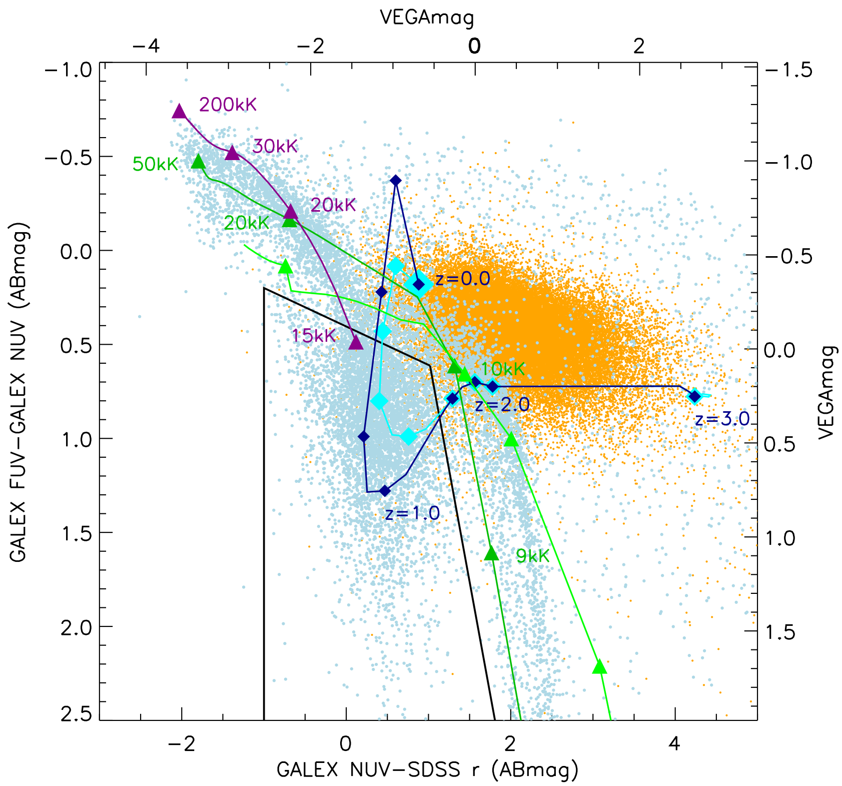

Figure 1. Objects from the combined SDSS–*GALEX* 2-color plane, from the catalog of Bianchi et al. (2010), showing the area selected for this sample of QSOs. The extended sources (orange: galaxies) occupy a distinct locus separate from most of the point sources (light blue). The loci of star and QSO templates are shown, main sequence (dark green), supergiants (light green), and white dwarfs (magenta). The QSO templates are for normal (cyan) and three times (dark blue) enhanced Lyα emission. The selected sample should be free of stars except for cooler white dwarfs.

Table 1
Average Measurements of Subsamples

Sample	No.	g[a]	NUV-i	g-FUV	g+i-2r (SD)
Spec QSOs	3895	19.1	0.93	−1.86	0.11 (0.22)
Spec stars	437	19.1	0.28	−1.62	0.03 (0.12)
Spec galaxies	78	18.9	1.27	−1.50	0.19 (0.49)
Ext photom	36770	21.4	1.21	−1.41	0.32 (0.74)
Point photom	22993	20.4	0.78	−1.58	0.10 (0.41)
Point phot—stars	19812	20.4	0.83	−1.62	0.11 (0.33)
Point QSO[b]	19100	20.4	0.84	−1.65	0.11

Notes.
[a] Median values for all photometry.
[b] Estimated without star contamination.

SDSS spectra, which we have used to characterize the larger photometric samples, which go to fainter limits. Table 1 shows the main properties of the samples and subsets discussed below.

Figure 2 shows the samples in the NUV-i/FUV–NUV plane. The spectroscopically identified subsamples show that the stars overlap little with the QSOs, while the galaxies do. However, as reported by Hutchings & Bianchi (2010), many of the spectroscopic "galaxies" are in fact QSOs, and they form a very small subsample in this two-color region. The distribution of the point source photometric sample covers the combined loci of the QSO and star sample, while the extended photometric sample has a different distribution, more resembling the true galaxy subgroup.

The "SED" using the 7 AB magnitudes offers another useful comparison between object types. Figure 3 shows this for the photometric samples compared with averages from various spectroscopic samples. The sequence of Lyα redshifted emission and shortward absorptions is clear for the redshift-binned QSOs, and the post-starburst galaxy mean (from Hutchings & Bianchi 2010) has a "dip" corresponding to the Balmer absorption continuum at the mean redshift of about 0.2. The stars are predominantly white dwarfs, from inspection of the spectra. We can see clearly that the point source photometric sample looks like a QSO of redshift about 0.8, contaminated with some stars, while the extended source plot looks very like the galaxy plot, possibly with some low redshift QSO contamination. Plots of the photometric samples separating bright and faint members at $g = 21$ are not significantly different. Thus, it appears that the fainter objects, which are in the photometric but not in the spectroscopic samples, are not systematically different.

2. STELLAR CONTAMINATION IN THE QSO SAMPLE

Before we go further with the QSO sample definition, we need to estimate the contamination of the point source sample by stars. Stars are about 10% of the spectroscopic sample. In Figure 2, those with NUV-i less than 0 comprise 30% of the stars and only 1.4% of the QSOs. If we examine this fraction as a function of g magnitude, it rises to about 38% for the fainter objects in the photometric catalog. The distribution of QSO values of NUV-i becomes slightly more positive as we go fainter, as expected from the models going to higher redshift. Thus, an estimate of the stellar contamination is about 2.6 times the number (1955) with NUV-i < 0 in the photometric catalog less than 1.4% (270) which are QSOs. This gives us an estimate of 4400 stars in the point source sample, or 19%.

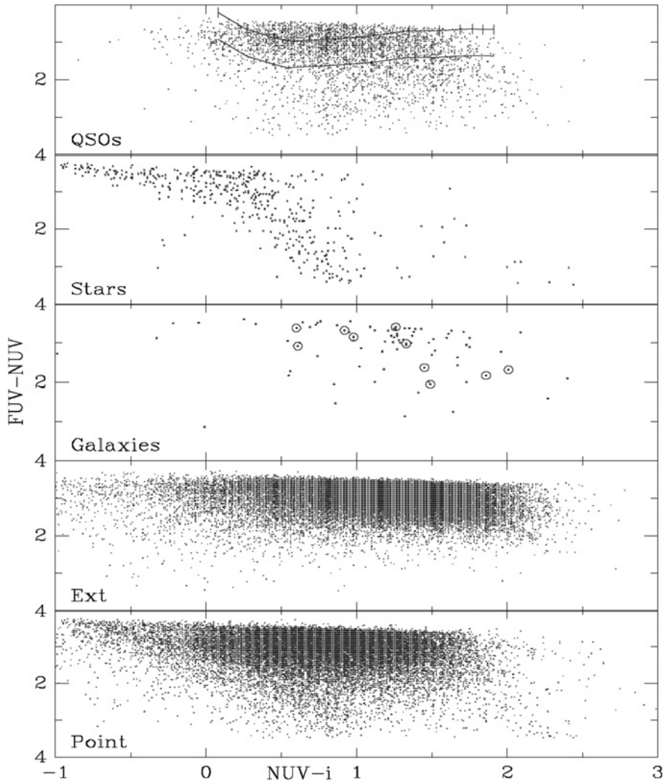

Figure 2. Subsamples discussed in 2-color plots. The top three panels show the objects with SDSS spectra, classified by the pipeline as labeled. In fact about half the "galaxy" spectra are QSOs. The circled galaxies are the superluminous starburst galaxies described by Hutchings & Bianchi (2010). The top panel shows models for QSOs tick marked from redshift 0.4 to 2.0, and a lower line that adds 1 mag of $E(B-V)$. The lower two panels show the photometric samples.

Another good separation of stars from QSOs is shown in Figure 4: the quantity $A = \mathrm{NUV}-3.5g+2.5i$. This is derived from a plot of NUV-g against $g-i$ where the separation gap has a linear slope of 2.5. In Figure 4 the population of stars is clearly separated, spreading as the photometric errors increase for the fainter stars. (In fact, there seems to be another small population of stars with A about 2.3.) A cut at $A = 1$ removes 3188 objects, which is most of the stars. A better number estimate is to count the objects with $A > 1.4$, representing a clean half of the spread of stars. This indicates that the true number of stars is 1937×2, or 3894, which is in good agreement with the 4400 estimated above. We thus assume a final QSO catalog with $A < 1$, of 19,800 objects, which should have only 700 stars (3.5%) as contaminants.

For a further sanity check on this, referring to Figure 5 (which we discuss in more detail below), the dotted contours are derived from the spectroscopic QSO sample. The number of spectroscopic stars in this region is 25 and the number of QSOs is 50. There are 250 objects in the point source sample in this region, so we deduce there are 80 stars, which scales to a total of 1400 stars in the whole sample. However, these are bright star counts, and the star density rises as we go fainter, so this is a lower limit, and correction for star density will raise that number by a factor of several. A plot of the spectroscopic stars in the g-FUV plane shows this, plus their distribution.

The full catalog of 19,812 point sources is available as an online table. It contains positions, all 7 magnitudes with formal errors, and a local $E(B-V)$ value for each, derived from the Schlegel et al. (1998) maps. Table 2 shows sample lines of the

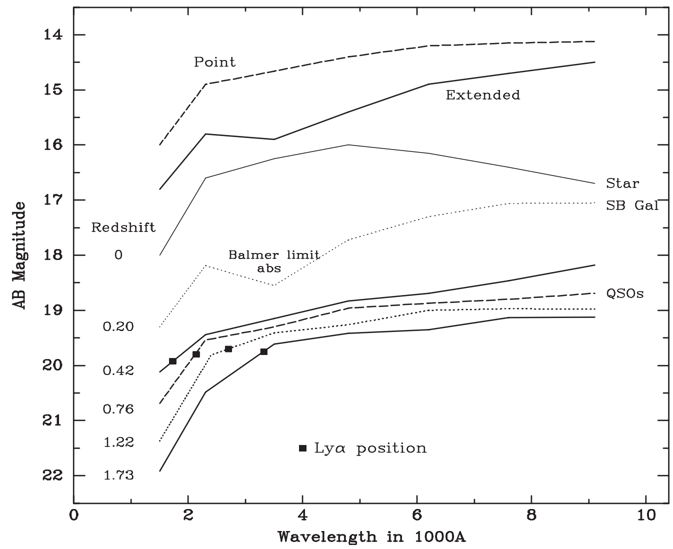

Figure 3. Median magnitudes for the various subsamples. The top plots are the photometric samples. The values for only the brighter objects ($g < 21$) are essentially the same, so there is no evidence that the fainter objects are different. The lower plots are from the spectroscopically identified subset. The sequence of redshifted QSOs is dominated by the position of the Lyα emission and Lyman absorption shortward of it. The SB galaxy spectrum is the mean of the luminous star-forming galaxies from the subset described by Hutchings & Bianchi (2010).

full table, which is ordered in R.A. with formal errors given in parentheses. The coordinates given are those from the SDSS.

3. REDSHIFT DISTRIBUTIONS

Figure 6 shows the redshift distribution of the spectroscopic sample of QSOs, lying, as expected from the color selection, in the redshift range 0.5–1.7. Since QSOs have a strong magnitude–redshift correlation, we split the group at $g = 19$ and find indeed that the fainter ones have higher mean redshift. If we normalize the redshift distributions to match the numbers in the whole spectroscopic sample, we find the excess distribution shown in Figure 6, for the fainter group. The brighter group has a similar excess at lower redshifts. Thus, we should expect the redshift distribution in the photometric sample, which goes fainter, to include more high redshift objects, within the limits imposed by the original color selection. We discuss the derivation of that distribution below.

As noted by Hutchings & Bianchi (2008), as well as in earlier papers by Richards et al. (2002) and Fan et al. (2000), the g, r, and i magnitudes provide some systematic color changes with redshift. In Figure 7 we show the change of a combined gri index for the spectroscopic sample, along with the QSO template values. The model matches the observations quite reasonably, and we find little change with reddening or Lyα flux, to the model. As noted by Hutchings & Bianchi (2010), inspection of the spectra shows that many of the "galaxy" samples (as classified by the SDSS pipeline) are QSOs, including the group at redshift 1.4. In addition, at the lowest redshift we have increasing host galaxy contamination, but the general behavior of the model still fits the data fairly well.

Since the gri index is multiple-valued with redshift, it does not provide an unambiguous redshift indicator and needs to be used with another. While there are color indices including the UV magnitudes that show monotonic change with redshift (see Hutchings & Bianchi 2008), there is a large scatter in all of them, which increases as we go to fainter objects. Instead, we

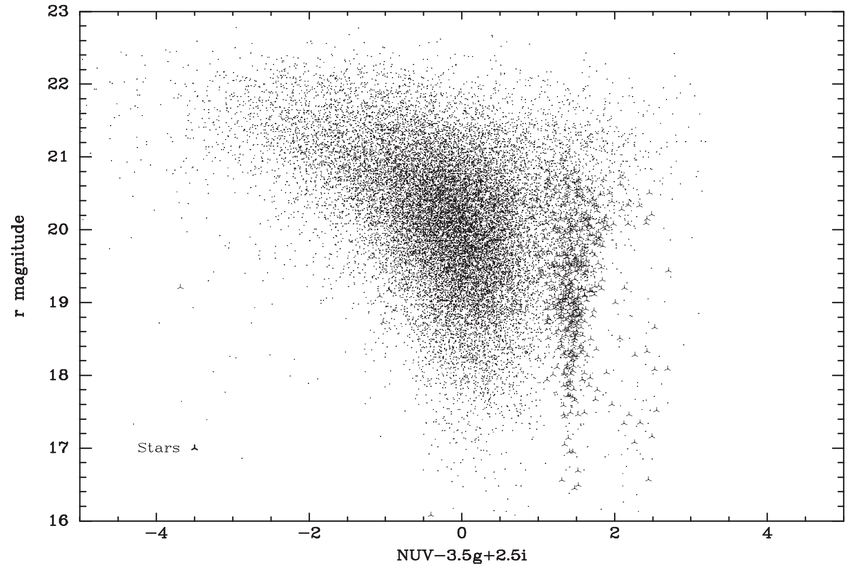

Figure 4. Separation of stars and QSOs using the three-color index of NUV, g, and i. The spectroscopically identified stars form a sequence at value 1.4, spreading as errors increase for fainter stars. The small dots are the entire point source photometric catalog. We discuss in the text how the stellar contamination is largely eliminated using this index.

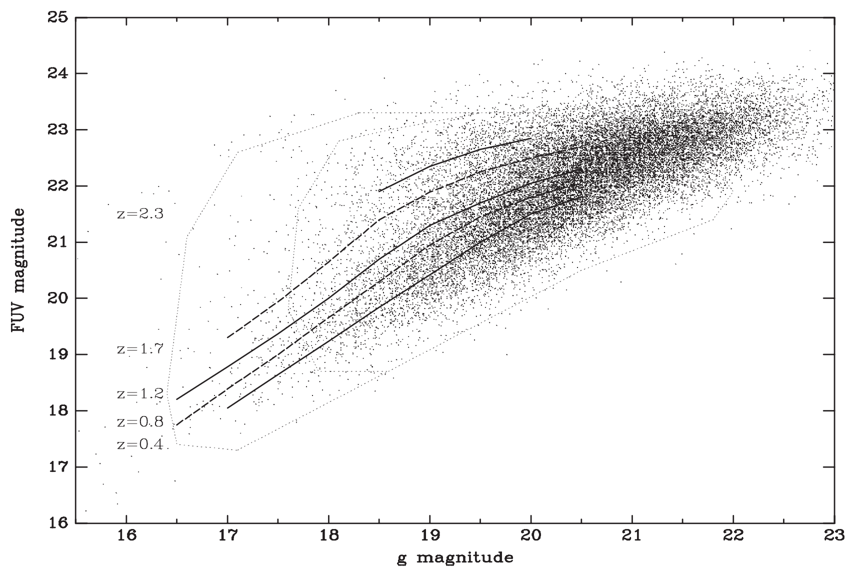

Figure 5. Point source photometric sample in the g-FUV plane. The lines are fits through the spectroscopic sample, in this plane, in redshift bins as labeled. The upper limit for fainter objects arises from the limiting FUV magnitude of the sample. While there is significant scatter, these relationships are used to estimate the redshift distribution of the photometric sample. The objects between the dotted "contours" are largely stellar contamination.

Table 2
Catalog of 19,812 QSO Candidates

R.A. (deg)	Decl. (deg)	FUV (err)	NUV (err)	u (err)	g (err)	r (err)	i (err)	z (err)	$E_{(B-V)}$[a]
0.0447922	−10.09915	22.79(0.24)	20.86(0.06)	21.15(0.23)	21.12(0.08)	20.64(0.10)	20.75(0.13)	19.87(0.38)	0.04
0.0482203	−10.12043	22.45(0.21)	20.82(0.06)	19.89(0.07)	19.69(0.02)	19.60(0.03)	19.54(0.04)	19.31(0.15)	0.04
0.0547671	14.17635	20.51(0.07)	19.52(0.03)	19.55(0.05)	19.31(0.01)	19.16(0.02)	19.24(0.03)	19.04(0.10)	0.06
0.0589557	−11.10500	21.85(0.14)	20.40(0.05)	20.66(0.13)	20.41(0.05)	20.26(0.06)	20.26(0.09)	20.12(0.32)	0.03
210.6115	4.878604	23.33(0.17)	22.08(0.15)	21.83(0.47)	21.34(0.10)	21.09(0.13)	20.61(0.12)	20.11(0.37)	0.03
210.6122	2.438051	21.12(0.10)	20.25(0.04)	20.08(0.08)	19.80(0.02)	19.80(0.03)	19.75(0.05)	19.90(0.26)	0.04
210.6293	5.482087	22.18(0.12)	21.07(0.05)	20.82(0.19)	20.25(0.04)	19.98(0.05)	19.92(0.08)	19.39(0.19)	0.03
210.6325	6.473025	21.78(0.14)	20.96(0.08)	20.77(0.12)	20.54(0.04)	20.51(0.06)	20.27(0.06)	19.89(0.17)	0.03

Note.
[a] Foreground extinction value, estimated from the Schlegel et al. (1998) maps.

(This table is available in its entirety in machine-readable and Virtual Observatory (VO) forms in the online journal. A portion is shown here for guidance regarding its form and content.)

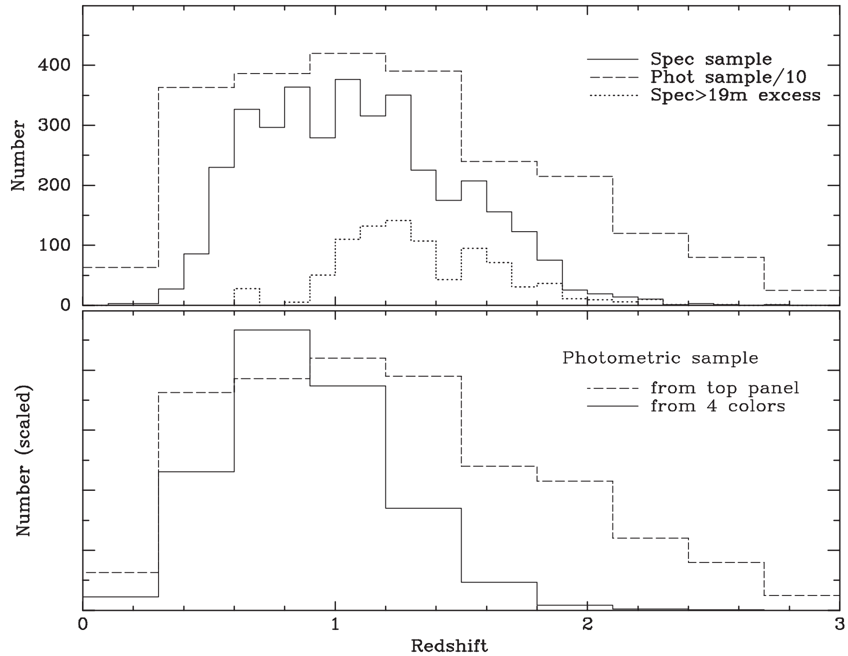

Figure 6. Redshift distributions in the samples. Upper: spectroscopically measured subsample and photometrically estimated full sample (see the text). The normalized difference between the full and fainter spectroscopic samples is the small histogram, which includes higher redshifts, as expected. The photometric sample also has fainter objects and shows a similar difference. Lower: comparison of the photometric redshift distributions from the upper panel and from a color–color plot.

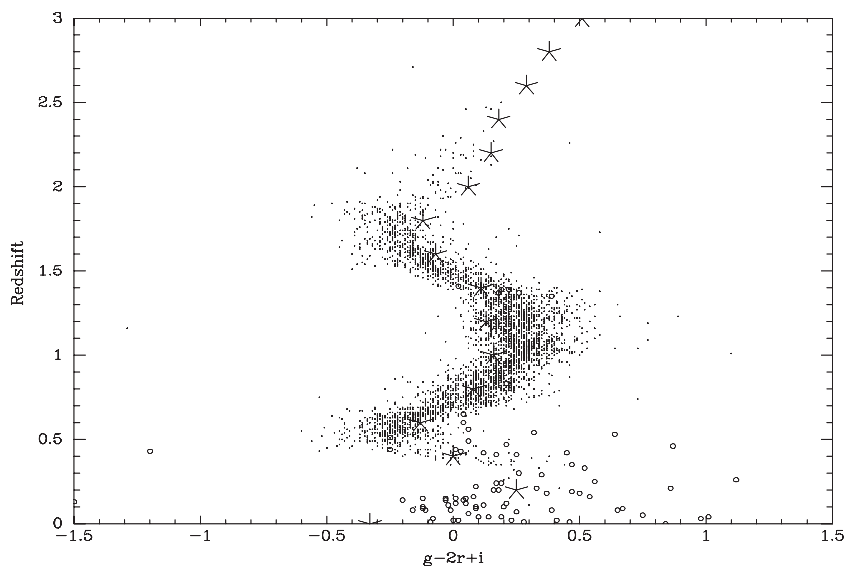

Figure 7. Systematic variation of *gri* colors with redshift. Dots are the spectroscopic sample and stars are the predictions for a standard QSO model. The circles are objects with spectra classified as galaxies, 25% of which we find to be QSOs, including the group at redshift near 1.4. Reddening of the spectrum has very little effect on the index at redshifts over 1.5, allowing us to assess the population at these redshifts in the photometric sample.

have used the plot of g against FUV, which is shown in Figure 5, for the point source sample. There is a broad correlation that is limited at faint magnitudes by the FUV flux limit, which becomes noticeable beyond 23.5. The spectroscopic sample is much less affected by this, and we find a systematic shift of the plot for QSOs in a series of redshift bins. Figure 5 shows the best-fit lines for the redshift bins labeled with their mean values.

At magnitudes brighter than $g \sim 20$, there is a fairly monotonic change in g-FUV with redshift, although there is a lot of scatter. For fainter magnitudes, the spread with redshift decreases, mostly due to losing objects as we run into the FUV flux limit. The distribution of *gri* values with redshift has maxima at values centered on −0.2 and 0.2, as can be seen in Figure 7. This shows up in plots of *gri* against g-FUV. At higher redshifts (i.e., generally fainter than the spectroscopic sample), the model shows this dichotomy spreading and including more positive values. Plots of the point source photometric sample show the same effect—the two peaks in *gri* are seen in the brighter subsample, but spread (and have lower g-FUV values) as we go fainter. This is all consistent with the point source sample being dominated by QSOs. The bright subsample also has a population with high (negative) g-FUV and *gri* value around 0.05. Referring to Figure 7, this indicates a small but significant population of bright QSOs with redshift in the range 2.0–2.4, which becomes visible in the larger sample.

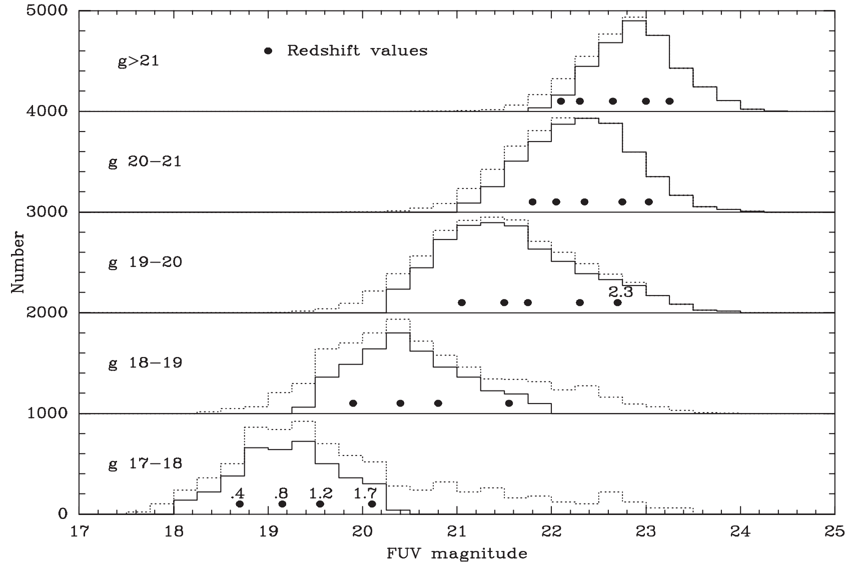

Figure 8. FUV magnitude (and hence redshift) distributions of the point source sample in bins of g-magnitude, derived from Figure 5. The dotted distributions are the full sample and the solid lines have the stellar contamination removed as described in the text. The dots as labeled show the mean FUV values for the labeled redshifts. The redshift distribution goes to higher values, as expected, for the fainter objects.

We note that the templates of Bianchi et al. (2009) predict the observed dependence of g-FUV with redshift, but with smaller values. The observed values of g-FUV are larger by a factor of about 1.5 overall. We discuss this point further below.

The extended source sample again behaves very differently from the point sources. Their g and FUV magnitudes are about a magnitude fainter and they lie beyond the QSO locus in the g/FUV plot. All our indications are that the extended source sample contains essentially no QSOs: it is dominated by faint galaxies with young populations at redshifts a few tenths or less. The extreme starburst galaxies discussed by Hutchings & Bianchi (2010) lie at the bright end of this population. Of the photometric sample, 5100, or 14% lie in the locus of our 10 extreme galaxies, and 360, or 1% overlap the brightest 4 of these. The "SED" plot for these and also the faintest members of the sample are essentially the same (Figure 3), so this appears to be a very uniformly populated sample of galaxies. The magnitude with the largest scatter (difference between mean and median) is the u-band, which is where the Balmer continuum absorption occurs at low redshift. In the faintest subset ($g > 23$ and FUV > 23) this begins to show up in the g-band too, suggesting that we are reaching slightly higher redshifts in the fainter galaxies.

We may now estimate the number and distribution in the g-FUV plane of stars in the point source catalog. In Figure 8, we show the distribution of FUV values for bins of g magnitude. The dotted lines are the total numbers, and the solid lines are the values corrected for star contamination. The solid distributions are assumed to be QSOs, and we have placed labeled dots at the mean values for the redshift bins from Figure 5. The histograms now show the distribution of redshift of the objects as we go fainter in g magnitude. The trend to higher redshift as we go fainter is evident. We note that the "calibration" and "sample" both suffer from the same FUV flux limits, so the result should be free of bias, although the scatter certainly will be larger than for the brighter objects.

If we combine the whole sample and derive the overall redshift distribution we get the result plotted in the lower panel of Figure 6. The larger population of higher redshift objects is evident compared with the brighter spectroscopic sample. We note again that the higher redshifts are truncated by the NUV-r color selection, which should eliminate those above 2.5 or so, as intended.

We have used a second approach to estimate the redshifts. In the spectroscopic sample, we find that NUV-u is correlated with redshift, although with large scatter. Plotting g-FUV against NUV-u gives a reasonable straight line fit, again with scatter. A rough estimate of redshift was made from this combined 4-color plot, for the point source photometric sample, calibrated by the spectroscopic sample. Figure 6 (lower panel) shows the redshift distribution derived this way. The two distributions do not agree very well, but the four-color distribution has not been corrected for the stellar contamination, which makes it less reliable. If we perform the same calculations on the stellar spectroscopic sample, we find the contaminating false redshifts lie mainly between 0.5 and 1.2, so statistical correction to these brings the distributions into better agreement (plotted in Figure 4, lower panel), but there is still a discrepancy above redshift 1.2.

4. LUMINOSITY

We have derived absolute magnitudes for the spectroscopic QSO sample by applying a distance modulus, plus a small foreground extinction correction based on the line of sight. The distance modulus is approximated by the expression 33.2+5(log(z))+4(log(z)+2)**2, for plots such as those by Gong et al. (2007). We apply no k-correction since there may be a range of intrinsic extinction and hence rest-frame color. An unreddened QSO spectrum has low k-corrections until it is sampled into the Lyman absorption wavelength range, which is redshift 3 in the g-band, and beyond our range of interest.

The spectroscopic sample mostly has an r-band limit of 19.4. However, about 20% of the QSO sample has r-band values down to 20.4. This allows us to judge completeness and to see the redshift distribution of the fainter sample. Figure 9 shows the redshift distributions for bins of absolute g-magnitudes. The dashed lines show the effect of going fainter. We can see which parts of the distributions are complete, from these plots.

We can also attempt a correction for completeness down to $r = 20.4$, by adding four times the difference, to achieve

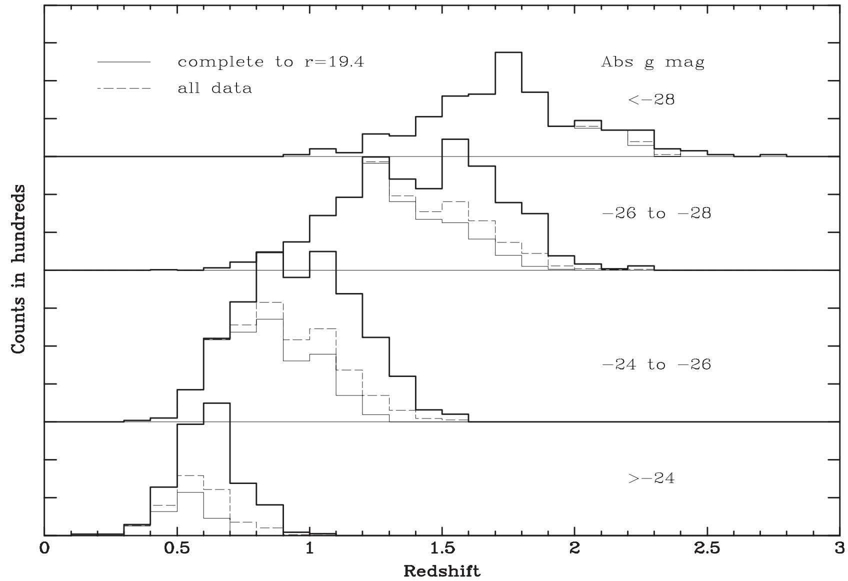

Figure 9. Redshift distributions of the spectroscopic sample in bins of absolute g-magnitude. The sample has a cutoff at $r = 19.4$, but a small subset goes to 20.4 (dashed lines). If we scale this difference to simulate the cutoff at 20.4 for all, we get the heavy solid lines. The diminishing incompleteness at higher redshifts can be judged for each luminosity bin and appears to be minimal for the highest luminosity objects, as expected.

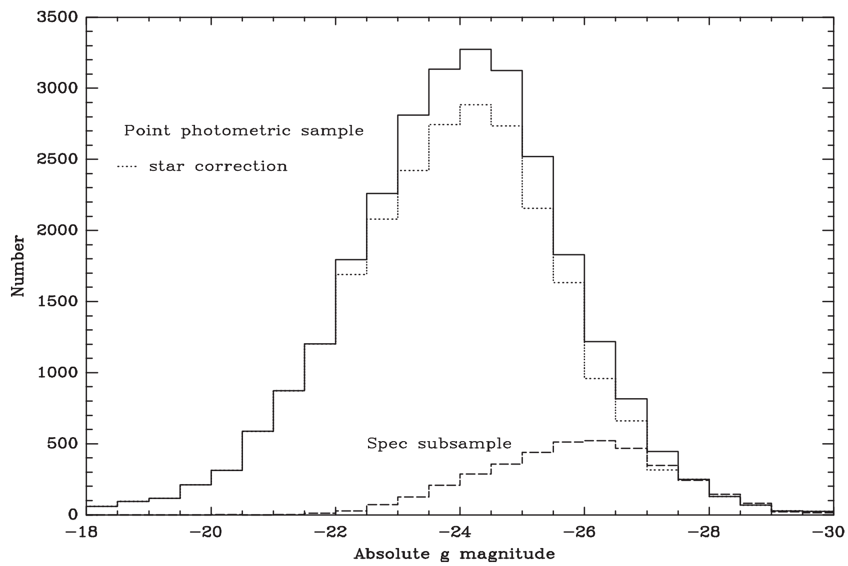

Figure 10. Distributions of absolute g-magnitudes for the spectroscopic and photometric samples, as discussed in the text. The dotted histogram shows the correction for stellar contamination in the photometric sample. The spectroscopic sample, as expected, contains higher luminosity QSOs.

the number counts we expect, extrapolating the spectroscopic number counts, and also referring to number counts with magnitude (e.g., Hutchings & Bianchi 2008). This gives us the heavy solid histograms in Figure 9. Completeness increases with luminosity and is very complete for the highest bin.

If we use the 4-color-derived values of redshift for the individual photometric sample objects, we get a distribution of absolute magnitudes, shown in Figure 10. This is after removal of the NUV-i values less than zero, which should eliminate 1/3 of the stars, and essentially no QSOs. We have plotted the spectroscopic distribution as well, scaled so that the high luminosity part of the distributions match, since we expect that the brighter limits of the spectroscopic sample will detect the most luminous QSOs. The scaling should be close to unity if this is true, and in fact is about 1.2, which is the amount of remaining star contamination expected as argued above. The distribution of contaminating false absolute magnitudes was estimated from the spectroscopic stellar sample, and lies mainly in the M_g range −23 to −26, which does not alter the comparison very significantly. As might be expected, the deeper photometric sample detects mostly lower luminosity QSOs. The good match in these numbers and distributions gives confidence again that the point source sample is almost entirely QSOs.

5. DISCUSSION

Overall, we consider that point sources with NUV-$i < 0$ are essentially all stars, so that our final QSO catalog consists of 19,812 objects, of which 19,100 are expected to be QSOs. The extended sources appear to contain essentially no QSOs.

The most extreme g-FUV values in the QSO catalog lie far below the models, in the sense of having fainter FUV magnitudes. This is true for the photometric and spectroscopic samples, but this red “tail” comprises 20% of the spectroscopic sample, 27%

in the bright ($g < 20$) spectroscopic sample, and 16% of the photometric sample, corrected for stellar contamination. The reddening required to cause this is up to 0.7 in $E_{(B-V)}$, with most of them 0.2 or less. As shown in Figure 1, this area is also populated by QSOs with unusually strong Lyα, when this moves into the NUV band (roughly 0.8–1.4). Spectroscopy of these objects will provide an interesting breakdown of these two subsets of QSOs. In the fainter photometric sample, we find fewer of these as we will lose objects with very faint FUV. Thus, the fraction of reddened or extreme Lyα QSOs has a lower limit of ∼30% in this redshift range.

Figure 2 shows models in the top panel that indicate that most QSOs have no reddening or even enhanced Lyα emission, but there is an interesting tail of objects with very faint FUV. If this is due to reddening, some 25% of QSOs have $E_{(B-V)} > 1$. However, the "SED" of these FUV-faint objects is essentially the same as the normal ones, except for the FUV magnitude, which does not suggest reddening—and certainly not this much. The FUV formal errors are similar, so the values have the same reliability. We are more likely seeing various amounts of Lyman absorption among the sample, which are not in our templates.

It is appropriate to question how this sample differs from catalogs produced from other selections from the SDSS alone. The latest example is the 7th data-release paper by Schneider et al. (2010), which includes 105,783 objects which are spectroscopically confirmed QSOs. Our catalog is based on seven-color photometry and is dominated by objects in the redshift range 0.5–1.5, with fainter limits. The spectroscopic sample is biased in redshift by the emission lines in the spectroscopic sample, while ours is based on a region of UV–optical color space that has few contaminants, and should have unbiased sampling of its redshift range.

The recent photometric catalog of QSO candidates based on SDSS data (Richards et al. 2009) is much larger, containing over a million objects, but also samples the redshift range less smoothly, and with significant aliases in the redshift range 0.5–1.5 (see their Figures 13 and 14). We did some comparisons with this catalog, as follows. We took several subsamples of the Richards et al. catalog, in different R.A. ranges, each of size some three times our sample in the R.A. range. The Richards et al. samples were restricted to the redshift range 0.5–1.5, to match our redshift range. We also estimated the relative sky coverage in the subsamples, from plots of R.A. and decl. for each. The results were the same for all subsamples—matching objects were found using the R.A. and decl. for all objects, with essentially no ambiguity, as checked by using a range of mismatch differences.

In all cases, about 50% of the objects in our catalog are found in the Richards et al. catalog. Between 15% and 40% of the Richards et al. objects are found in ours. The latter number depends on the relative sky coverage estimates. The explanation for these numbers comes from two selection differences. First, our catalog is restricted to sources with photometric errors less than 0.3 mag in *GALEX* and SDSS bands, to isolate the clean area in our color diagram in Figure 1. The Richards et al. catalog has a cutoff at $i = 21.3$. The result is that our sample includes fainter objects, and this is verified by histograms of the g and i magnitudes for the subsamples. We also find that the matching objects are the brighter ones from each. If we do the match only on objects with $i < 20$, the match rate is over 90% of our objects.

There are further differences. Our sample is made up from *GALEX* surveys, with different magnitude limits, so that the Richards et al. sample is more complete in the magnitude range just below their $i = 21.3$ cutoff. Our sample also may reject real candidates based on our position match criterion between the *GALEX* and SDSS catalogs. The overall total size of the samples does not match the relative overall sky coverage (8417 and 1103 deg^2) for the same reasons. There is a factor 2.5 for redshift range restriction, and another 2.5 for the various selections and rejections noted. All of these points muddy any exact comparison of the samples. However, we consider the comparison is consistent with the claims of purity of both samples, so that they serve different purposes. Our sample has a very high purity of QSOs, based on the selection criteria (see especially Figure 4), and includes more objects, based on the *GALEX* colors, but has selection biases different from the Richards et al. sample. Put another way, our sample doubles the number of QSOs in the Richards et al. catalog, in the areas of overlap, mostly by going deeper.

Improved photometric classification and redshift determination is of interest as many large surveys exist and are in planning. The addition of far-UV adds usefully to the sampling of QSOs in this redshift range (about 0.5–1.5), and our 96% catalog efficiency may be of use in correcting redshift uncertainties or biases that exist in ground-based photometry. The UVIT instruments on board the ISRO Astrosat observatory should be a powerful new tool for extending such sample selections, having more filters and several times higher resolution than *GALEX*.

We thank Boryana Efremova and James Herald who helped build the original catalogs of Bianchi et al. (2010) from which this sample was extracted. This work is based on archival data from the NASA *Galaxy Evolution Explorer* (*GALEX*) which is operated for NASA by the California Institute of Technology under NASA contract NAS5-98034. We thank the referee for helping improve the presentation of the paper.

Facilities: GALEX, Sloan

REFERENCES

Bianchi, L. 2009, Ap&SS, 320, 11
Bianchi, L., et al. 2009, AJ, 137, 3761
Bianchi, L., et al. 2010, MNRAS, submitted
Fan, X., et al. 2000, AJ, 119, 1
Gong, Y., Wang, A., Wu, Q., & Zhang, Y.-Z. 2007, J. Cosmol. Astropart. Phys., JCAP08(2007)018
Hutchings, J. B., & Bianchi, L. 2008, PASP, 120, 275
Hutchings, J. B., & Bianchi, L. 2010, AJ, 139, 630
Richards, G. T., et al. 2001, 122, 1151
Richards, G. T., et al. 2002, AJ, 123, 2945
Richards, G. T., et al. 2004, ApJS, 155, 257
Richards, G. T., et al. 2009, ApJS, 180, 67
Schlegel, D. J., Finkbeiner, D. P., & Davis, M. 1998, ApJ, 500, 525
Schneider, D. P., et al. 2010, arXiv:1004.1167